Proceedings of the
47th IEEE Conference on Decision and Control
Cancun, Mexico, Dec. 9-11, 2008

Neural-based Control of Modular Robotic Fish with Multiple Propulsors

Yonghui Hu, Wei Zhao, Long Wang, and Yingmin Jia

Abstract— **This paper presents a neural-based control method for a modular robotic fish with a pair of two-degree-of-freedom pectoral fins and a tail fin. A central pattern generator (CPG) model that consists of a network of neural oscillators (NOs) is utilized to generate the target joint angle. The properties of NO network and basic strategies of joint angle control is numerically investigated. Through the coordinated control of the propulsors, a diversity of swimming patterns are implemented. Experiments are conducted to validate the effectiveness of the proposed method.**

I. INTRODUCTION

Biorobotic autonomous underwater vehicles (BAUV) have become an active research field in the last few years [1]. The use of biologically-inspired propulsion and maneuvering mechanisms can bring several advantages over the conventionally used screw type propellers, such as high efficiency, great agility, increased noise reduction, and so on. With the increasing understanding of the swimming mechanisms of aquatic animals and the progress in material, sensor, control and fabrication technologies, the nautical technology that we have been acquainted with will be revolutionized in the future.

As one of the most common aquatic animals, fish have received considerable attention from both the biological and engineering communities for their excellent swimming performances. The evolutionary Darwinian process of "natural selection" guarantees that the body morphology, fin design and locomotory style of fish are nearly optimal for their specific habitat. Based upon the propulsive structures employed for locomotion, the swimming of fish can be classified into two categories: body and/or caudal fin (BCF) swimming and median and/or paired fin (MPF) swimming [2]. BCF swimmers generate thrust by bending their bodies into a backward moving propulsive wave that extends from the nose to caudal fin. The variation in wavelength and the amplitude envelope of the propulsive wave further split the BCF swimming into several subcategories, from anguilliform swimming that involves the undulation of the whole body, the carangiform swimming in which the undulation is confined to the last third of the body length, to the ostraciiform swimming characterized by the pendulum-like oscillation of the caudal fin. The MPF swimming is also categorized into different types according to the propulsors that contribute to thrust generation and the extent to which propulsion is based upon undulatory versus oscillatory motion.

Recent years have seen the emergence of various swimming machines that mimic the morphology and locomotion of fish. The pioneering work on fish-like robot was performed by Triantafyllou who built the well-known RoboTuna and experimentally validated its effectiveness of drug reduction in 1994 [3]. Subsequent successful robotic fish include the mission-scale, autonomous underwater vehicle VCUUV by Anderson and Kerrebrock [4], the pectoral fin driven robotic fish "BlackBass" by Kato [5], the behavior-based robotic fish by Liu *et al.* [6], the fin-actuated agile maneuvering robotic fish by Morgansen *et al.* [7], the undulating fin mechanism by Low [8], *et al.*. Excellent reviews regarding the state of art biomimetic robotic fish are provided in [9].

The objective of this paper is to present a neural-based swimming control method for a modular robotic fish with multiple propulsors. The robotic fish is constructed with several waterproofed function modules allowing structure reconfiguration. A pair of two-degree-of-freedom (2DOF) pectoral fins, as well as the oscillating caudal fin are utilized to generate the propulsion and maneuvering forces. Neurophysiological studies have shown that the rhythmic movements in locomotion, such as walking, running, swimming and flying are controlled by central pattern generators (CPGs), which are neuron networks that produce coordinated oscillatory signals in the absence of sensory input or descending inputs from higher cognitive elements [10]. The biologically inspired neural-based method allows online gait generation of the swimming locomotion. Compared with trajectory-tracking method that generates joint angle command according a prescribed reference trajectory, the neural-based method enables smooth transitions between gaits, allows integration of sensory feedback, and demonstrates adaptation to both perturbations in the environment and modifications of the control parameter.

The rest of the paper is organized as follows. Section II briefly introduces the mechatronic design of the robotic fish prototype. Section III addresses the neural-based control of swimming locomotion and several swimming patterns are designed based on coordinated control of the propulsors. Swimming performances of the robotic fish are experimentally evaluated in section IV. Finally, concluding remarks for this paper are provided in section V.

This work was supported by National Natural Science Foundation of China (10372002, 060505015), National 863 Program (2006AA04Z258), NSFC (60674050 and 60528007), National 973 Program (2002CB312200), and 11-5 project (A2120061303).

Yonghui Hu, Wei Zhao, and Long Wang are with Intelligent Control Laboratory, Center for Systems and Control, Department of Mechanics and Space Technologies, College of Engineering, Peking University, Beijing 100871, P. R. China (e-mail:yonghhu@pku.edu.cn; huyhui@gmail.com)

Yingmin Jia is with the Seventh Research Division, Beihang University, Beijing 100083, P. R. China

978-1-4244-3124-3/08/$25.00 ©2008 IEEE

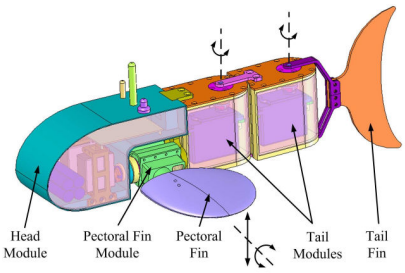

Fig. 1. Mechanical configuration of the robotic fish.

II. MODULAR ROBOTIC FISH PROTOTYPE

The robotic fish is composed of a head module, a pair of pectoral fin modules and two tail modules. To generate the propulsive and maneuvering forces, a wing-like pectoral fin is attached to each pectoral fin module and a crescent-shaped tail fin to the rear tail module. The number of tail module can be adjusted according to which kind of swimming the robotic fish is aimed to mimic, for example, one for ostraciiform and five or more for anguilliform swimming. In this case, two tail modules are adopted to form a carangiform swimming robotic fish. The head module provides housings for the power and electronics. Two R/C servomotors Futaba S9451 are fixed symmetrically at the bottom of the head module, and the rotating shafts connected with the servomotors run through dynamic sealing structure filled with grease backwardly to provide the heaving motion of the pectoral fins. The pectoral fin modules are placed symmetrically at the rear lower position of the head module and are supported on both sides of the semi-cylindrical part. A R/C servomotor Futaba S3103 sits in the interior cavity of pectoral fin module and the rotation of the servomotor is referred to as the pitching motion of the pectoral fin. Each tail module encapsulates a R/C servomotor Hitec HS-755HB for body deflection of the robotic fish. The head module and the tail modules are interconnected sequentially by mechanical linkage. The anterior tail module is screwed to the head module and the rotating shaft of each tail module is connected to its hinder element with mechanical linkage, allowing relative rotation between elements. Fig. 1 shows the mechanical configuration of the robotic fish.

The modular robotic fish is designed for free swimming. Four rechargeable Ni-Cd cells of 2500mAh capacity provide the robotic fish about one hour power autonomy. The control unit is the microcontroller AT91SAM7A3 that incorporates a high-performance ARM7TDMI core running at 48MHz and a wide range of peripherals from ATMEL Corporation. A dual axis accelerometer ADXL202 is used to measure the accelerations in the pitch and roll axes. The controller connects a RF module through UART port for radio control and measures the duty cycle of the PWM signal generated by the accelerometer. Six PWM signals are generated by the microcontroller to control the motion of the joints. Table I summarizes the technical specifications of the modular robotic fish prototype.

TABLE I
SPECIFICATIONS OF MODULAR ROBOTIC FISH PROTOTYPE

ITEM	VALUE
Dimension (L × W × H)	460mm × 270mm × 280mm
Weight	2.2kg (with 2 tail modules)
Microcontroller	AT91SAM7A3, 48MHz
Actuator	R/C Servomotor
Power Supply	DC, 4.8V, 2500mAh
Operation Mode	Radio Control, 444MHz
Sensor	Dual Axis Accelerometer

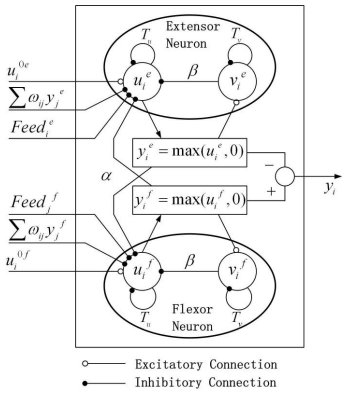

Fig. 2. A neural oscillator with two mutually inhibiting neurons.

III. LOCOMOTION CONTROL OF ROBOTIC FISH

A. Neural Oscillator Model

The locomotion of vertebrate animals is characterized by the coordinated alternation of flexion and extension of muscles. Such rhythmic motor patterns are produced by the activities of complex networks of neurons located in the spinal cord known as CPGs [11]. The intrinsic membrane properties of the neurons that form the network and the properties of the synaptic connectivity among them determine the behavior of these networks. By providing sensory feedback and descending inputs from higher cognitive elements, the timing characteristics of the CPG can be modulated and as a result different motor behaviors can be generated. The appealing features of CPGs include the learning ability of adapting their operation to a variety of body and environment changes, and the potential to lead to distributed, thus fault-tolerant and robust, motion control architectures.

Ichthyology studies reveal that rhythmic patterns of neural activity exist in both the motion of fin systems and the axial motion of fish body [12]. Base on this knowledge, the mathematical model of CPG originally formulated by Matsuoka [13] is adopted and introduced into the swimming gait generation of the robotic fish. As illustrated in Fig. 2, the CPG is modelled as a neural oscillator (NO) that consists of an extensor neuron and an flexor neuron with mutually inhibitory connections. Each neuron receives tonic input that drives neuron oscillation, inputs from other neurons and sensory feedback signals. The dynamics of the NO is governed by the following nonlinear differential equations

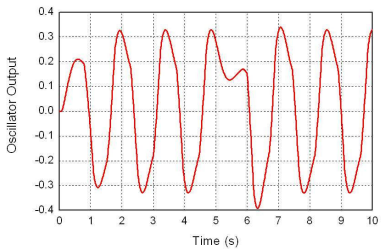

(a) Disturbance rejection property.
When $5 \leq t \leq 6$, $Feed_i^e = 0.5$, $Feed_i^f = 0$; otherwise $Feed_i^e = 0$, $Feed_i^f = 0$.

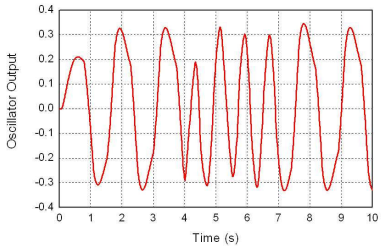

(b) Entrainment to cyclic external input signal.
When $4 \leq t \leq 7$, $Feed_i^e = max(0.8sin(8t), 0)$, $Feed_i^f = max(-0.8sin(8t), 0)$; otherwise $Feed_i^e = 0$, $Feed_i^f = 0$.

Fig. 3. Typical output of the neural oscillator. Parameters: $T_u = 0.3$, $T_v = 0.6$, $\beta = 5$, $\alpha = 2$, $u_i^{0e} = 1$, $u_i^{0f} = 1$, $\forall j, \omega_{ij} = 0$.

that exhibit limit cycle behavior:

$$T_u \dot{u}_i^e = -u_i^e - \beta v_i^e - \alpha y_i^f - \sum_{j=1}^{n} \omega_{ij} y_j^e - Feed_i^e + u_i^{0e} \quad (1)$$

$$T_v \dot{v}_i^e = -v_i^e + y_i^e \quad (2)$$

$$T_u \dot{u}_i^f = -u_i^f - \beta v_i^f - \alpha y_i^e - \sum_{j=1}^{n} \omega_{ij} y_j^f - Feed_i^f + u_i^{0f} \quad (3)$$

$$T_v \dot{v}_i^f = -v_i^f + y_i^f \quad (4)$$

$$y_i^{\{e,f\}} = max(u_i^{\{e,f\}}, 0) \quad (5)$$

$$y_i = y_i^f - y_i^e \quad (6)$$

where u_i^e and u_i^f are inner states of the extensor and flexor neurons of the ith NO, respectively; v_i^e and v_i^f are variables representing the degree of the self-inhibition effect of the neurons; y_i^e and y_i^f are outputs of extensor and flexor neurons; u_i^{0e} and u_i^{0f} represent tonic excitation that modulate the amplitude of the oscillator output; β is a constant representing the degree of the self-inhibition influence on the inner state; T_u and T_v are time constants characterizing the output wave shape and its frequency; α is a connecting weight between flexor and extensor neurons; ω_{ij} indicates the connecting weight between neurons of the ith and jth NO; $Feed_i^e$ and $Feed_i^f$ are sensory feedbacks from the robotic fish; y_i is the output of the ith NO.

The equations describing the NO model can not be solved analytically. The mathematical conditions to achieve stable oscillations are analyzed in [13], and the relationship between the parameters and the oscillator output is numerically explored in [14]. An attractive characteristic of NO is that it can adapt to external sensory input, and the output can return to its original oscillation after the incoming signal is removed. In addition, when an oscillatory input signal is applied, the NO can entrain the input, locking onto the input frequency. Fig. 3 shows typical simulated outputs of the NO, demonstrating its disturbance rejection and entrainment properties.

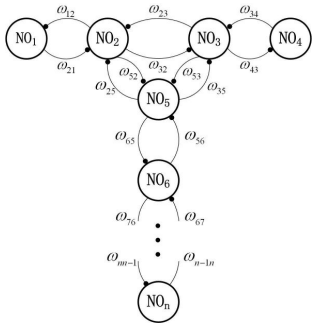

Fig. 4. Structure of the neural oscillator network. The NOs numbered as 1,2,3,4,5,...,n correspond to left pitching joint, left heaving joint, right heaving joint, right pitching joint, the first tail joint, ... , and the $(n-4)$th tail joint, respectively.

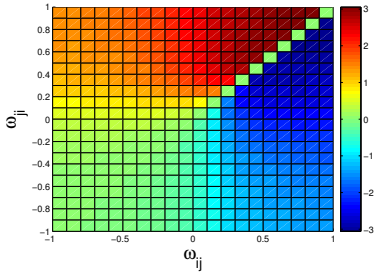

Fig. 5. Relationship between phase difference and connecting weights. Parameters: $T_u = 0.3$, $T_v = 0.6$, $\beta = 5$, $\alpha = 2$, $u_i^{0e} = 1$, $u_i^{0f} = 1$, $u_j^{0e} = 1$, $u_j^{0f} = 1$, $Feed_i^e = 0$, $Feed_i^f = 0$, $Feed_j^e = 0$, $Feed_j^f = 0$.

B. Neural Oscillator Network for Fish-like Swimming

Each joint of the robotic fish is allocated with a NO, whose output is used as the target joint angle. To generate fish-like swimming with the modular robotic fish, the neural oscillations of the joints should be coordinated by assigning appropriate coupling and synaptic strength between NOs. A NO network, which is illustrated in Fig. 4 is built to perform inter-joint coordination. To simplify the structural complexity of the network, only neighboring NOs are connected. By coupling the joints, the NOs are mutually entrained and oscillate in the same period with a fixed phase difference.

The effective generation of thrust by either the tail fin or the pectoral fins requires specific phase shift between joints to be maintained. For two interconnected NOs, the phase difference mainly depends on the connecting weights between them. The relationship between the phase difference

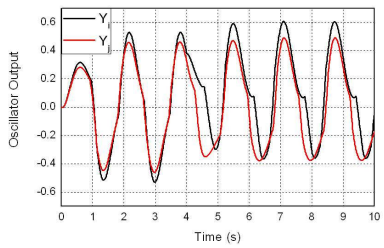

Fig. 6. An implementation example of angle bias. When $t < 4$, $u_i^{0e} = 1$, $u_i^{0f} = 1$, otherwise $u_i^{0e} = 0.6$, $u_i^{0f} = 1.4$. Other parameters: $T_u = 0.3$, $T_v = 0.6$, $\beta = 5$, $\alpha = 2$, $u_j^{0e} = 1$, $u_j^{0f} = 1$, $Feed_i^e = 0$, $Feed_i^f = 0$, $Feed_j^e = 0$, $Feed_j^f = 0$, $\omega_{ij} = -1$, $\omega_{ji} = -0.6$.

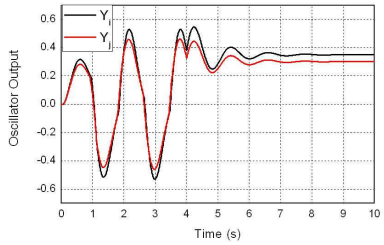

Fig. 7. An implementation example of oscillation suppression. When $t < 4$, $u_i^{0e} = 1$, $u_i^{0f} = 1$, $u_j^{0e} = 1$, $u_j^{0f} = 1$, otherwise $u_i^{0e} = 0.2$, $u_i^{0f} = 1.8$, $u_j^{0e} = 0.4$, $u_j^{0f} = 1.6$. Other parameters: $T_u = 0.3$, $T_v = 0.6$, $\beta = 5$, $\alpha = 2$, $Feed_i^e = 0$, $Feed_i^f = 0$, $Feed_j^e = 0$, $Feed_j^f = 0$, $\omega_{ij} = -1$, $\omega_{ji} = -0.6$.

and the connecting weights is numerically investigated. A series of simulations is carried out with the connecting weights ω_{ij} and ω_{ji} each varying from -1 to 1. From Fig. 5, it can be concluded that the phase difference depends on the quadrant in which the point $(\omega_{ij}, \omega_{ji})$ locates. The plane is split into two symmetric areas by the line $\omega_{ij} = \omega_{ji}$, on which the phase difference is zero meaning synchronous oscillation of the two NOs. In the area where $\omega_{ij} > \omega_{ji}$, the oscillation of the ith NO lag that of the jth NO in phase. The phase difference falls into the range of $(-\pi, 0)$ and is narrowed as the weights decrease. The same tendency is observed where $\omega_{ij} < \omega_{ji}$, except that the phase difference is in the range of $(0, \pi)$.

Angle bias of the rotating joint is essential to the aquatic maneuvering of the robotic fish. We achieve angle bias by applying different tonic excitations to the extensor and flexor neurons, which in biology innervate corresponding motor neurons connected with muscles. Fig. 6 shows an example of implementing angle bias. As illustrated in the figure, the output wave of the NO is biased towards the neuron with larger tonic input. It is also noticeable that its adjacent NO is slightly affected through mutual coupling.

Another control demand for the swimming locomotion of the robotic fish is to produce static offset deflection of the joint. Simulation studies suggest that the oscillation of the NO can be suppressed when tonic inputs to the extensor and flexor neurons differ drastically. Fig. 7 shows an example of oscillation suppression. The successful realization of oscillation suppression requires that adjacent NOs don't oscillate due to the entrainment properties of the NO.

C. Implementation of Swimming Patterns

Based on the proposed NO network and the above joint angle control strategies, a great diversity of fish-like swimming patterns can be realized. Here we investigate basic BCF and MPF swimming patterns as well as hybrid swimming patterns that require simple coordination of the propulsors.

(1) **BCF forward swimming:** The robotic fish swims in a straight line by actuating the tail joints, while the pectoral fins are held parallel to the horizontal plane. To realize this pattern, the tonic excitation of the pectoral fins and the connecting weights associated with them are set to be zero. Because the thrust is generated by bending the body into a backward moving propulsive wave, the rhythmic oscillation of each tail joint should lead its succeeding joints in phase.

(2) **BCF turning in advancing:** Unequal tonic excitations are applied on the NO of the tail joint to produce angle bias, while the other parameters remain the same as the BCF forward swimming.

(3) **BCF sharp turning:** The robotic fish first attains a relatively high swimming speed with BCF forward swimming and suddenly bends the body into a "C" shape by driving the joints at the tail to their angular limits. The posture holds for a short period of time and then switches back to its original swimming behavior. The oscillation suppression strategy is used here to generate static joint deflection of the tail.

(4) **MPF forward and backward swimming:** This swimming behavior can be achieved by the synchronized movements of the paired pectoral fins, with the body and caudal fin held straight. To generate anteriorly directed thrust, the phase differences between the heaving NO and the pitching NO are in the range of $(0, \pi)$. For phase differences in the range of $(-\pi, 0)$, backward swimming can be accomplished. The parameters on one side should equal the corresponding parameters on the other side in order for the thrust on both sides to be equal.

(5) **MPF turning:** The differentiation of hydrodynamic forces between the pectoral fins will cause a yawing moment that is necessary to execute turning maneuvers on the fish body. An effective method to produce the yawing moment is to produce anteriorly directed force on one side and posteriorly directed force on the other side.

(6) **Submerging and ascending:** Three-dimensional motion is achieved by adjusting the attack angle of the pectoral fins, which can be realized through offsetting the pitching joint with oscillation suppression. As a precondition, the robotic fish should attain a higher swimming speed with BCF forward swimming pattern. The attack angle of the pectoral fin on each side should take the same value in order not to generate yawing or rolling moments.

(7) **Braking:** The robotic fish brakes through sudden rotation of the pectoral fins to a position perpendicular to the body. The drag caused by the pectoral fin decelerates and eventually stops the motion of the robotic fish.

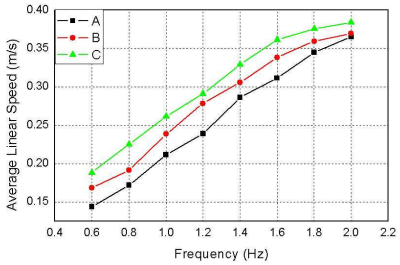

Fig. 8. Average linear speed in BCF forward swimming with different frequencies and amplitudes. The amplitudes used in each case are: $A = \{A_5 = 10°, A_6 = 20°\}$, $B = \{A_5 = 20°, A_6 = 30°\}$, $C = \{A_5 = 30°, A_6 = 40°\}$.

IV. EXPERIMENTAL RESULTS

To verify the feasibility and effectiveness of the proposed control methods, several experiments are carried out in an indoor swimming tank of 2250mm $\times$ 1250mm $\times$ 350mm. The robotic fish is marked with specified colors and the information within the swimming tank is captured by an overhead CCD camera. The image is transmitted to a PC and processed with a visual tracking software platform developed to obtain the position and orientation of the robotic fish in real time. The two dimensional trajectory of the robotic fish can also be extracted and recorded for post-analysis.

Experiments with the robotic fish are conducted by testing the swimming patterns described above. The nonlinear differential equations that describe the NO network include dozens of parameters, which precludes the possibility of a thorough exploration. Since there is no explicit relationship between the parameters of the NO network and the swimming kinematics, i.e. angular offset, oscillatory frequency, amplitude and phase shift of the joints, simulations are carried out before the experiment to determine the suitable parameters that generate the desired joint motion. The swimming performance is tested by varying the concerned kinematic parameter while holding the others constant.

For BCF forward swimming pattern, the average linear speed is tested by varying the tail beat frequency f_t and the amplitude of the first tail joint A_5 and the second tail joint A_6. Three groups of amplitudes are employed while the frequency is varied in each case. The phase shift used to generate the travelling wave is $\frac{\pi}{2}$. The swimming speed, as illustrated in Fig. 8, increases almost linearly with the frequency and large amplitude can also provide more thrust. Due to the open-loop property of motor control system, the desired amplitudes can not be reached at higher frequency, which results in the speed saturation at the performance limits of the servomotors. The maximum speed of BCF forward swimming can reach 0.38 m/s, which is approximately 0.82 body length per second.

The swimming performance of BCF turning in advancing can be evaluated in terms of turning radius R and turning rate ω. The angular offsets have been chosen as the principal parameter for test, although other parameters have been believed to have, but not such a strong influence on the turning performance. The turning radii and turning rates of this swimming pattern with four angular offsets added to each of the tail joints are listed in table II. According to the experimental results, the turning radius decreases and the turning rate increases with the increase of the angular offsets, so that this behavior can be used not only for small course adjustment but also for rapid turn in narrow space.

TABLE II

SWIMMING PERFORMANCE OF BCF TURNING IN ADVANCING. THE AMPLITUDES ARE $A_5 = 20°$, $A_6 = 30°$, AND THE OSCILLATORY FREQUENCY OF TAIL FIN IS $f_t = 1Hz$.

Anglular offsets (deg)	10	20	30	40
R (m)	1.26	0.94	0.69	0.36
ω (rad/s)	0.49	0.66	0.85	1.09

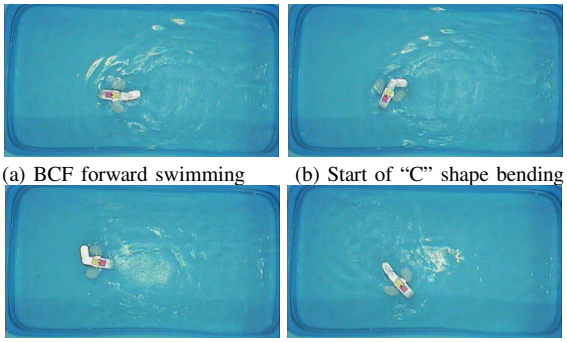

(a) BCF forward swimming (b) Start of "C" shape bending

(d) Hold the posture (f) Straighten the body

Fig. 9. Snapshots of BCF sharp turning.

In the experiment of BCF sharp turning, the robotic fish swims straight to reach an initial speed of 0.3m/s. The "C" shape posture lasts for 2.8s before robotic fish straightens its body. Fig. 9 shows a series of snapshots during this swimming pattern. By employing BCF sharp turning, the robotic fish can achieve a heading change as large as 120°.

Tests of MPF-based straight swimming patterns are carried out by varying the frequency, while the amplitudes are kept at constant values and the phase difference is held at $\frac{\pi}{2}$ on both sides for forward swimming and $-\frac{\pi}{2}$ on both sides for backward swimming. Fig.12 shows the forward and backward swimming speeds at different frequencies. As BCF forward swimming, the speeds increase in proportion with the frequency in both cases. However, for the same frequency, the speed of backward swimming is significantly less than that of forward swimming, which can be explained by the fact that the pitching motion occurs at the quarter chord position of the pectoral fin.

In MPF turning, we employ the same kinematic parameters on both sides, except the phase shift which is $\frac{\pi}{2}$ on one side and $-\frac{\pi}{2}$ on the other side. The turning performance is tested under different frequencies. The experimental results are shown in table III. As shown in the table, the turning radius increases with higher frequency, while the turning rate remains almost constant under different frequencies.

The accelerometer is used in submerging to measure the

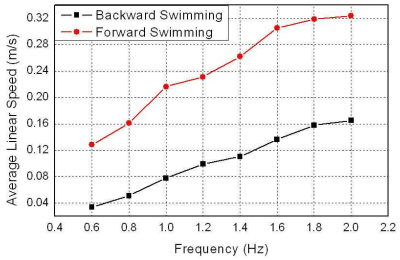

Fig. 10. Average linear speed in MPF forward and backward swimming. The amplitudes used in both cases are: $A_1 = 30°$, $A_2 = 40°$, $A_3 = 30°$, $A_4 = 40°$.

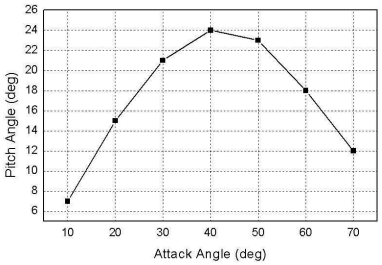

Fig. 11. Relationship between the attack angle of pectoral fins and the pitch angle of fish head.

TABLE III

SWIMMING PERFORMANCE OF MPF TURNING. THE AMPLITUDES ARE: $A_1 = 30°$, $A_2 = 40°$, $A_3 = 30°$, $A_4 = 40°$.

Frequency (Hz)	0.6	1.0	1.4	1.8
R (m)	0.44	0.61	0.79	0.97
ω (rad/s)	0.31	0.34	0.33	0.32

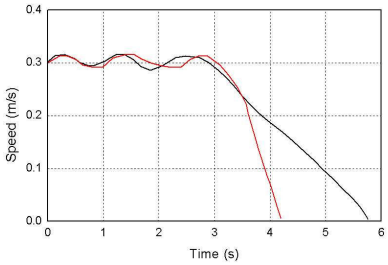

Fig. 12. Speed records in inertia drift and braking. The BCF forward swimming ends at $t = 3s$.

pitch angle of the fish head, which determines the descending speed of the robotic fish. BCF forward swimming with tail beat frequency of 1.5Hz is employed to provide the forward speed in the test. The relationship between the attack angle of pectoral fins and the pitch angle of fish head is shown in Fig. 11. The pitch angle increases at small attack angle and decreases when the attack angle is larger than $40°$. The drop in pitch angle is caused by slow forward speed at large attack angle, which induces considerable drag on the pectoral fins.

The effectiveness of braking is validated by comparing the deceleration rate of stopping with and without this swimming pattern. Before braking is executed, the robotic fish accomplished a swimming speed of 0.3 m/s with BCF forward swimming. Fig. 12 shows the speed records in inertia drift and braking. As shown in the figure, the deceleration rate of the robotic fish is significantly elevated with braking.

V. CONCLUSIONS

The online generation of fish-like swimming based on CPG brings an array of advantages in addition to the disturbance rejection property mentioned above. The neural-based method allows dynamical change of the swimming kinematic parameters without causing jerks that may damage the servomotors. Smooth transitions between swimming patterns, which can not be realized with sine-based method are also made possible. The main drawback of this method is the lack of systematic methodology to set the parameters for a desired output. Online optimization with genetic algorithm can be conducted to find the parameters that produce the most effective swimming.

This paper was concerned with neural-based control of a modular robotic fish with a pair of 2DOF pectoral fins and a tail fin. A CPG model consisting of a network of NOs was utilized for swimming locomotion control and several swimming patterns were designed based on the coordinated control of propulsors. Experimental results demonstrated the effectiveness of the proposed methods.

REFERENCES

[1] P. R. Bandyopadhyay, "Trends in biorobotic autonomous undersea vehicles," *IEEE J. Oceanic Eng.* **30**(1), 109-139 (2005).
[2] M. Sfakiotakis, D. M. Lane, and J. Bruce C. Davies, "Review of fish swimming modes for aquatic locomotion," *IEEE J. Oceanic Eng.* **24**(2), 237-252 (1999).
[3] M. S. Triantafyllou and G. S. Triantafyllou, "An efficient swimming machine," *Sci. Amer.* **272**(3), 64-70 (1995).
[4] J. M. Anderson and P. A. Kerrebrock, "The vorticity control unmanned undersea vehicle (VCUUV)-An autonomous vehicle employing fish swimming propulsion and maneuvering," *Proc. 10th Int. Symp. Unmanned Untethered Submersible Technology*, 189-195 (1997).
[5] N. Kato, "Control performance in the horizontal plane of a fish robot with mechanical fins," *IEEE J. Oceanic Eng.* **25**(1), 121-129 (2000).
[6] J. Liu, H. Hu, and D. Gu, "A hybrid control architecture for autonomous robotic fish," *Proc. Int. Conf. Intelligent Robots and Systems*, 312-317 (2006).
[7] K. A. Morgansen, B. I. Triplett, D. J. Klein, "Geometric methods for modeling and control of free-swimming fin-actuated underwater vehicles," *IEEE Trans. on Robot.* **23**(6), 1184-1199 (2007).
[8] K. H. Low, "Locomotion consideration and implementation of robotic fish with modular undulating fins: analysis and experimental study," *Proc. Int. Conf. Intelligent Robots and Systems*, 2424-2429 (2006).
[9] J. E. Colgate, K. M. Lynch, "Mechanics and control of swimming: a review," *IEEE J. Oceanic Eng.* **29**(3), 660-673 (2004).
[10] E. Marder and D. Bucher, "Central pattern generators and the control of rhythmic movements," *Current Biol.* **11**, 986-996 (2001).
[11] S. Grillner, "Locomotion in vertebrates: central mechanisms and reflex interaction," *Physiological Review* **55**, 247-304 (1975).
[12] F. A. Mussa-Ivaldi and S. A. Solla, "Neural primitives for motion control," *IEEE J. Oceanic Eng.* **29**(3), 660-673 (2004).
[13] K. Matsuoka, "Mechanisms of frequency and pattern control in the neural rhythm generators," *Biological Cybernetics* **56**, 345-353 (1987).
[14] M. Williamson, "Neural control of rhythmic arm movements," *Neural Networks*, **11**(7-8), 1379-1394 (1998).